COB09-2890 - SPHERE-PLAN CONTACT OF METAL-POLYMER: HERTZ MODEL x EXPERIMENT

Isaac Vinícius do Nascimento, isaac882006@yahoo.com.br
Laís Vasconcelos Silva, laisvasc@gmail.com
Jarbas Santos de Medeiros, jarbas_inf@yahoo.com.br
Ruthilene Catarina Lima da Silva, ruthilene@ufrnet.br
João Telésforo Nóbrega de Medeiros, jtelesforo@yahoo.com
Universidade Federal do Rio Grande do Norte - **UFRN**, **PPGEM**, Group of Tribology Studies – GET, Natal – RN - Brazil

Abstract. *Structural sliding parts of metal-polymer have amplified their industrial applications due to low cost and noise, good functionality and tribological performance features. The aim of this work is to compare the theoretical footprints obtained by the Hertzian model of a set of sphere-plan contacts and the experimental footprints obtained due to the quasistatic contacts of a metal and viscoelastic materials. A sphere of 52100 heat treated steel of 6,35 mm diameter was used to promote indentations in the plan surfaces of five polymers: NBR, PTFE graphited, PTFE+MoS_2, polyurethane (PU) and a polymeric composite. The polymer samples were grinded with #100 to #500 sandpapers, minimizing the surface roughness and residual stress dispersions of these surfaces. The sphere was fixed to a bench drill press and submitted to normal loads of 9, 45, 90 and 135 N. For each normal load, there were seven indentations, resulting 28 scars, that were geometrically characterized. To measure the contact scars were used magnifying lens (40X) and a micrometer. The theoretical values of the Hertzian Contact parameters (the scar geometry, Hertz's contact pressure and shear stress distribution) were obtained using an Excel® spreadsheet. The elastic properties were obtained from the DMA testings (Young's modulus of polymers,* $\boldsymbol{E_{polym}}$*) and literature (Poisson ratios* $\boldsymbol{\nu_{polym}}$, $\boldsymbol{\nu_{steel}}$ and $\boldsymbol{E_{steeb}}$*) The experimental and theoretical mean values of the contact diameter,* ***2a*** *were compared after the application of these four different normal loads. The experimental measurements were larger than the expected theoretical values for all polymeric materials. These relations (measured values/expected theoretical values) were monotonically crescent with the normal load growth. This phenomenon was attributed to viscoelasticity features of the polymers. These aspects are discussed based on the experimental evidences and current literature.*

Keywords*: 1-Contact Mechanics; 2-Hertz Contact Pressure; 3-Polymer; 4-52100 Steel.*

1. INTRODUCTION

The use of tribological pairs of polymer-metal surfaces used by structural parts is crescent in the industry. Their applications are due to excellent characteristics of mechanical properties and high performance, that differentiate them of other groups of materials, like slideways and seals since the biomedical and food processing industry until the petroleum Engineering and parts developed for human prosthesis and artificial organs. Nowadays, there are milliards of types of polymers, naturals or composites, manufactured for universal or specific industrial applications.

Most of the polymers are viscoelastic. They present an elastic component, with a spring function (energy storage) and a viscous component, with a damping function (energy dissipation). This behaviour justifies their intense application to systems where it is necessary a good damping and high deformations and describes a dependant behaviour of time, load and temperature, which is related to the stress and strain actuating in the materials submitted to contact under a normal load. Figure 1 shows two different representations for the viscoelastic features of polymers (models of (a) Voigt-Kelvin and (b) Maxwell).

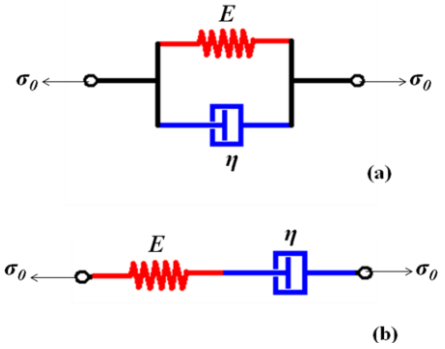

Figure 1. Two different models of viscoelastic materials submitted to a constant normal stress (a) model of Voigt-Kelvin, and (b) steady creep, model of Maxwell (Johnson, 1989).

In the current context, the objectives of this work are (a) evaluate the experimental values of the scar dimensions from indentations made in some polymers using a metallic sphere and (b) compare them with the theoretical values of the Hertzian model, the classic pioneer of the Contact Mechanics.

1.1 Contact Mechanics: Hertz's Theory

According to Johnson (1989), the first appear of the subject *contact mechanics* was in 1882, with the publication of the article "On the contact of elastic solids", by Heinrich Hertz. It was questioned if the elastic deformation of glass lenses under the action of a normal force that kept them in contact could have a significant influence on the standard of the interference fringes. (It was questioned if once under action of the force that keeps them in contact, the elastic deformation of glass lenses could have a significant influence on the standard of the interference fringes.)

Hertz studied the contact between two elastic solids with profiles of smooth surface (without roughness) which could be approached as a parabola near the contact area (see figure 2). This theory predicts that the contact area, **A** increases non-linearly with the squeezing force **F**, but as **A** is proportional to $\mathbf{F}^{2/3}$ (Persson, 2006). Hertz made some assumptions based on comments that the contact area has elliptical shape for such three-dimensional bodies.

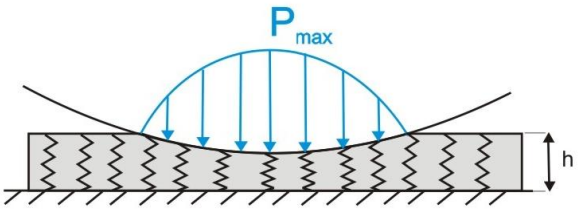

Figure 2. Sketch of the contact pressure distribution ***p*** on the contact area based on the elastic model with a rigid base of depth ***h*** that is squeezed by a rigid indentator (based in Johnson, 1989).

Hertz (1882) evidenced in his modelling, that the contact pressure ***p*** assumes the form of an elastic field potential with a well defined boundary. Inside this field, the stresses are associated to the elastic deformations. Beyond the field boundary, the elastic deformations in both the solids due to the contact are zero (Medeiros, 2002). Figure 3 shows the contact pressure distribution of the Hertzian model in three dimensions and the geometrical magnitudes of the deformations, **a** and **b,** at the Cartesian axles **x** , **y** , respectively, characterizing an elliptical contact area.

The important contribution of Hertz was to demonstrate mathematically that, in contact, static solids non-conformal squeezed itself and without friction, *geometric features* and *elastic properties* of the two materials are necessary and enough to define the *surface contact area* and the correlate surface and subsurface *stress and deformation states*.

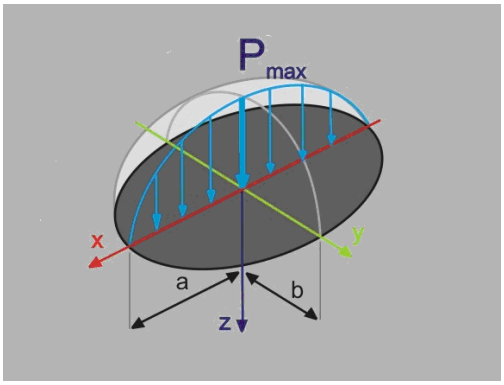

Figure 3. Hertzian parameters (contact ellipse *radii* **a, b**, distribution curve and maximum contact pressure $\mathbf{P_{max}}$) due to a non-conformal contact between two squeezed solids loaded by a normal force **F** (based on Norton, 1996).

When two structural bodies with a plain, concave or convex surface enter in contact under a defined normal load, these two surfaces deform themselves giving forms to a small contact area. The deformations may be either elastic or plastic, depending on the magnitude of the applied normal load and the material's elastic properties. In many Engineering applications as rolling bearings tracks, gears, cams, seals, the contacting surfaces are non-conformal and the resulting contact areas are very small and, as a consequence, the resulting pressures are very high (Stachowiak and Batchelor, 2005). These stresses can be determined from the analytical formulae, based on the theory developed by

Hertz for elastic deformations. They are simplified when the contact area is applied for spheres or sphere-plan in contact. Figure 4 presents a sketch of the contact area between a sphere and a plan, its respective geometry and the contact pressure distribution on the basis at the Hertz theory.

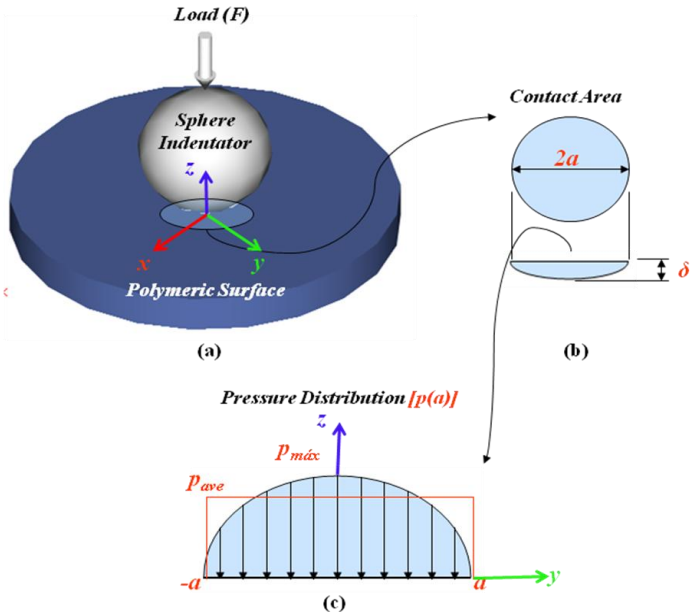

Figure 4. (a) Contact between two solids in the sphere-plan configuration under the action of the squeezing force **F** **(b)** contact area diameter, **2a** and approach
(c) contact pressure distribution, maximum($p_{máx}$) and average (p_{avg}) contact pressures ($p_{máx}$ = 3/2 p_{avg})

1.1.1. Contact Pressure and Area on the Sphere-Plan Contact Configuration

Figure 4 presents the contact pressure distribution for a sphere-plan contact configuration. The parabolic equation that describes the Hertzian contact pressure distribution as an elastic response of the surfaces is given by (Johnson, 1989):

$$p = p_{máx}\,(1 - (x^2/a^2))^{1/2} \qquad (1a)$$

which maximum is

$$p_{máx} = 3/2\; p_{avg} = [3/2\;(F/\pi a^2)] \qquad (1b)$$

where a is the contact area radius and, on the basis the Hertz contact mechanics theory, is given by the expression:

$$a = [(3FR/4E)^{1/3}] \qquad (2)$$

R is the equivalent radius of curvature in contact, $1/R = (1/R_{sphere} + 1/R_{flat})$. The *radii* of the sphere and the plan are, respectively, R_{sphere} and R_{flat}. The plan radius R_{flat} is considered infinite or very bigger than the sphere radius R_{sphere}, i.e., $R_{flat} \rightarrow \infty$ or $R_{flat} >> R_{sphere}$. E is the equivalent elasticity modulus of the two bodies in contact, and considering, respectively, the Poisson ratio the sphere and the plan; E_{sphere} and E_{flat} and the Young's modulus of both materials,

$$1/E = [((1- \nu_{\text{sphere}}^2)/E_{\text{sphere}})+((1- \nu_{\text{flat}}^2)/E_{\text{flat}})],\ \nu_{\text{sphere}} \text{ and } \nu_{\text{flat}} \qquad (3)$$

Under the action of a constant normal force, the height of penetration due to the indentation will grow with the time while the contact pressure will decrease (Johnson, 1989). Figure 5 shows four profiles of the contact pressure distribution and the associated growth of the contact area with the time.

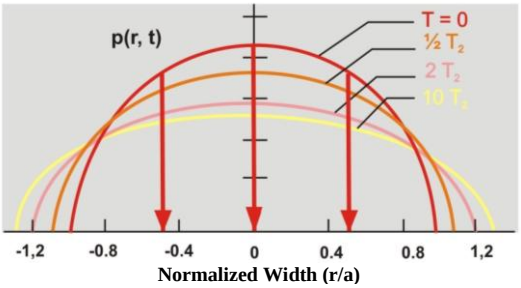

Figure 5. Variation at the contact area and contact pressure distribution with the time when a constant force is applied to a metallic sphere that indent a viscoelastic solid (based in Johnson, 1989).
P(r,t) is the Hertzian contact pressure as a function of the contact radius, ***a*** and the time, ***t***.

1.1.2 Static Stress Distributions in a Spherical Contact

The pressure on the contact patch creates a three-dimensional stress state in the material. The three applied stresses σ_x, σ_y and σ_z are compressive and are maximal at the sphere surface in the center of the patch. They diminish rapidly and nonlinearly with the depth and with the distance from the axes of contact (Norton, 1996). These stresses are called the Hertz stresses. Considering that axle Z increases with the depth in the material, these equations can be given by:

$$\sigma_z(z) = p_{máx}\,[-1 + (z^3/(z^2 + a^2)^{3/2})] \quad (4a)$$

$$\sigma_x(z) = \sigma_y(z) = (p_{máx}/2)\,[-(1+2v) + 2(1+v)((z/(a^2 + z^2)^{1/2}) - (z/(a^2 + z^2)^{1/2})^3] \quad (4b)$$

where σ_x, σ_y and σ_z are, respectively, the compressive stresses that act in the direction of axes X, Y and Z due to the action of the compression normal load **F**; ***z*** is the depth, considering its beginning from the contact interface.

For the calculation of the shear stress distribution, the maximum shear stress and the position where it occurs are used the equations

$$\tau(z) = (p_{máx}/2)\,[((1-2v)/2) + (1+v)((z/(a^2 + z^2)^{1/2}) - (3/2)(z/(a^2 + z^2)^{1/2})^3] \quad (5a)$$

$$\tau_{máx} = (p_{máx}/2)\,[((1-2v)/2) + (2/9)(1+v)((2(1+v))^{1/2})] \quad (5b)$$

$$z_{\tau_{máx}} = a[(2+2v)/(7-2v)]^{1/2} \quad (6)$$

Figure 6 shows the distributions of the normal stresses σ_x, σ_y and σ_z and the shear stress τ for depth z.

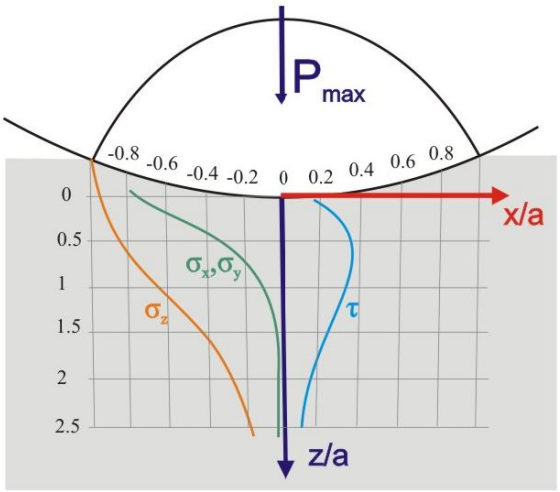

Figure 6. Normalized stresses distributions σ_x, σ_y and σ_z and the shear stress τ along the z axis in Static spherical contact (based in Norton, 1996).

The normal stresses induce the shear stresses. In this case, its maximum value occurs at a depth **z = 0.*63a*** in each material. This value varies in accordance with the Poisson ratio of the material. The calculation of the maximum shear stress and its position in the subsurface are sufficiently significant in the study of surface fatigue failure. The theory says cracks that begin below the surface eventually grow to the point that the material above the crack breaks out to form a pit (Norton, 1996). Pits and microspallings of this nature were experimentally verified by Medeiros, 2002.

2. MATERIALS AND METHODOLOGY

The polymeric materials used in this study were: NBR (Nitrile-Butadiene Rubber), PU (Polyurethane), PTFE+G (Polytetrafluorethylene graphited), PTFE+kaolin+MoS_2 (Polytetrafluorethylene +kaolin+ MoS_2), and a polymeric composite composed of PTFE, PEEK, carbon fiber and graphite (TECAPEEK®). Table 1 presents the elastic properties of these materials, whose elasticity modulus were obtained through dynamic mechanical analysis (DMA) at ambient temperature 30°C and the Poisson ratios ***ν*** of the site *Matweb.com*.

Table 1. Elastic materials property: Young modulus **E** and Poisson ratio ***ν***.

Materials	**Young Modulus E(Pa)**	**Poisson Ratio *ν***
NBR	0.0254×10^9	0.5
PU	0.0650×10^9	0.45
PTFE + G	1.1042×10^9	0.3
PTFE + Kaolin + MoS_2	1.5956×10^9	0.25
TECAPEEK	3.6246×10^9	0.4

The coupons were cylinders (diameter 40.0±0.5mm, height 11.5±1.5mm). The surfaces were grinded with #100 to #500 SiC sandpapers. The sphere was fixed in a bench drill press, Figure7, and this system was utilized to carry out the indentations for different loads. Carbon papers, 100μm thickness (Dentistry application), a 52100 heat treated steel sphere, 6.35 mm diameter (indentator), a magnifying lens (40X) and a micrometer (10 μm resolution) were used. Figure 7 illustrates the procedure adopted in this investigation.

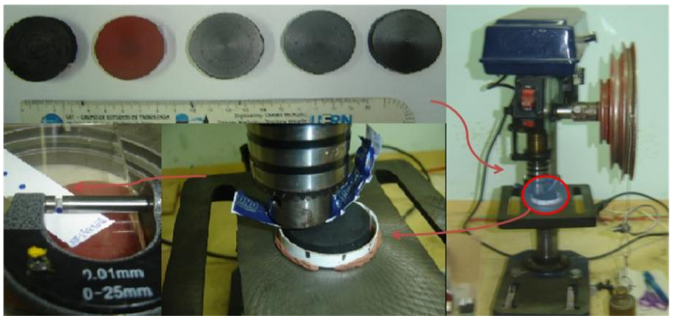

Figure 7. Procedure of the indentation, materials, grinding of the coupons, bench drill press, lens and micrometer.

It were made seven indentations, circumferentially distributed and at 1.0±0.5 mm of the edge on a same surface for each load in each coupon and for all polymeric materials, calculating the respective values of mean, median and standard deviation of the contact diameter dimension (**2a** contact parameter). Figure 8 illustrates this adopted procedure.

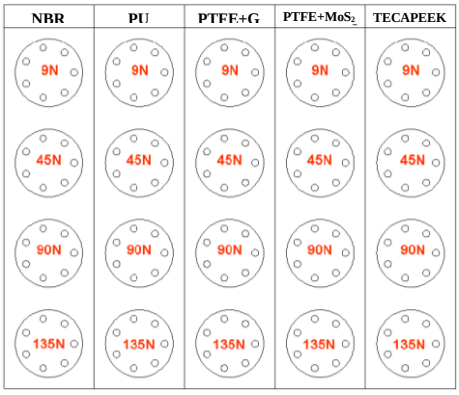

Figure 8. Schema of the indentation distribution and normal load applied to the coupons

3. RESULTS

3.1. Contact Area Dimension

Table 2 presents the mean values of the theoretical and experimental results obtained for the *contact diameter* parameter (**2a**) for the tested materials. The theoretical values were calculated using an Excel® sheet using the Hertz contact theory applied to sphere-plan configuration. The values of the material elastic properties and features of the contact are shown in Table 1. As the sphere radius $\boldsymbol{R_{sphere}}$ = 1/8'' = 3.175mm can be considered that $\boldsymbol{R_{flat}}$ >> $\boldsymbol{R_{sphere}}$, it was used for the calculations $\boldsymbol{R_{flat}}$ = 1000x $\boldsymbol{R_{sphere}}$, for a reasonable convergence of the results.

Table 2. Theoretical and experimental results for *indentation mean diameters* (**2a**) measured in the polymer surfaces for normal loads of **9 N**, **45 N**, **90 N** and **135 N**

MATERIALS	LOAD [N]	*HERTZ THEORY [mm]*	*EXPERIMENT [mm]*
NBR	*9*	1.72	2.18
	45	2.94	4.42
	90	3.70	5.83
	135	4.23	6.55
PU	*9*	1.32	1.66
	45	2.26	2.89
	90	2.85	3.86
	135	3.26	4.47
PTFE+G	*9*	0.52	1.12
	45	0.89	1.77
	90	1.12	2.28
	135	1.29	2.56
PTFE+Kaolin+MoS_2	*9*	0.47	1.13
	45	0.80	1.74
	90	1.00	2.17
	135	1.15	2.44
TECAPEEK®	*9*	0.34	1.02
	45	0.59	1.32
	90	0.74	1.46
	135	0.85	1.53

The graphs plotted in the Figure 9 reveal important differences theory x experiments for the materials like rubber (NBR and PU) and polymers (PTFE+G and PTFE+kaolin+MoS_2). The ***y*** axis of the graphs for the rubber has different amplitudes because the parameters *normal load* (that varied a magnitude order) and *contact diameter* **2a** reveal substantive information about the viscoelastic and viscoplastic responses of a same material and between different polymeric materials. These results reinforce the comments of the literature about caution for the Hertz theory applied to the viscoelastic materials. The differences in the values of the standard deviations plotted must be also observed.

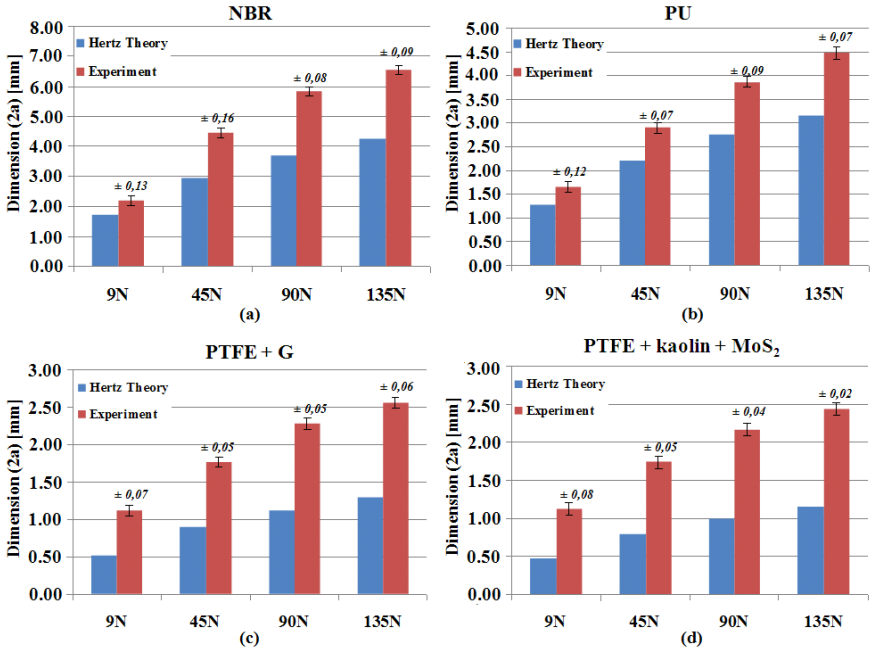

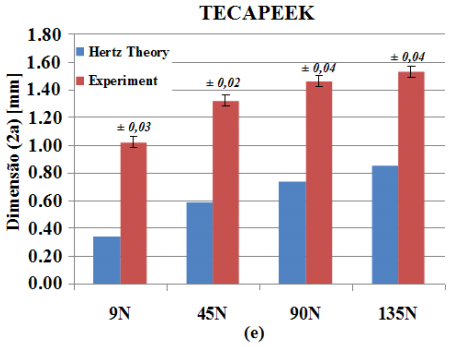

Figure 9. Theoretical and experimental results of the contact indentation diameter to the squeezing forces of 9N, 45N, 90N and 135N for (a) NBR, (b) PU, (c) PTFE+G, (d) PTFE+kaolin+MoS_2 and (e) TECAPEEK®

In accordance with the results presented in the Figure 9, for the polymers tested, the values of the Hertz theory approached to the experimental values for a load of 9N. With the increase of the load applied it was noticed a tendency to nonlinear deviation between theoretical and experimental values. Due to their chemical features and mechanical properties, the elastomeric materials NBR and PU were that presented greater value of contact dimension (2a), i.e., they deformed more. This behaviour is related with the low modulus of elasticity (low stiffness) of these materials and a high value of its viscous component compared with the elastic component.

The composite polymeric matrices (PTFE+G, PTFE+Kaolin+MoS_2 and TECAPEEK®) presented a difference of the experimental contact dimensions values smaller than the elastomers NBR and PU compared to those obtained by the Hertz modeling. As these materials have Young's modulus higher than the elastomers, they present smaller contact dimensions, being the minors gotten in the contact with the TECAPEEK®.

The biggest dispersions were gotten with elastomers NBR and PU, but relatively low comparatively to their contact diameters. The same happened with the polymeric composites, whose dispersions were still smaller.

3.2. Contact Pressure Distribution

Table 3 presents the values of the *maximum contact pressure* and their respective contact diameters that originate them, calculated by the Hertz theory. The contact indentation diameter **2a** are those calculated according to this theory and experimentally obtained in laboratory.

Table 3. Results of the maximum pressures and its respective theoretical and experimental contact areas with loads of 9N, 45N, 90N and 135N for **(a)** NBR, **(b)** PU, **(c)** PTFE+G, **(d)** PTFE+kaolin+MoS_2 and **(e)** TECAPEEK®.

NBR			
Experiment		*Hertz Theory*	
2a [mm]	$p_{máx}$ [Pa]	2a [mm]	$p_{máx}$ [Pa]
9N			
2.18	3.62E+06	1.72	5.83E+06
45N			
4.42	4.40E+06	2.14	9.97E+06
90N			
5.83	5.06E+06	2.70	1.26E+07
135N			
6.55	6,01E+06	4.23	1.44E+07

(a)

PU			
Experiment		*Hertz Theory*	
2a [mm]	$p_{máx}$ [Pa]	2a [mm]	$p_{máx}$ [Pa]
9N			
1.66	6.24E+06	1.28	1.05E+07
45N			
2.89	1.03E+07	2.20	1.79E+07
90N			
3.86	1.15E+07	2.76	2.26E+07
135N			
4.47	1.29E+07	3.16	2.58E+07

(b)

PTFE+G			
Experiment		*Hertz Theory*	
2a [mm]	$p_{máx}$ [Pa]	2a [mm]	$p_{máx}$ [Pa]
9N			
1.12	1.37E+07	0.52	6.32E+07
45N			
1.77	1.74E+07	0.89	1.08E+08
90N			
2.28	3.31E+07	1.12	1.36E+08
135N			
2.56	3.93E+07	1.29	1.56E+08

(c)

PTFE+kaolin+MoS_2			
Experiment		*Hertz Theory*	
2a [mm]	$p_{máx}$ [Pa]	2a [mm]	$p_{máx}$ [Pa]
9N			
1.13	1.35E+07	0.47	7.90E+07
45N			
1.72	2.84E+07	0.80	1.35E+08
90N			
2.17	3.65E+07	1.00	1.70E+08
135N			
2.44	4.33E+07	1.15	1.95E+08

(d)

TECAPEEK®			
Experiment		*Hertz Theory*	
2a [mm]	$p_{máx}$ [Pa]	2a [mm]	$p_{máx}$ [Pa]
9N			
1.02	1.65E+07	0.34	1.46E+08
45N			
1.32	4.93E+07	0.59	2.49E+08
90N			
1.46	8.06E+07	0.74	3.14E+08
135N			
1.53	1.10E+08	0.85	3.60E+08

(e)

On the basis of the values shown in Table 3 and using the Equation 1a, it was plotted the graphs of the Figure 10. They present the theoretical and experimental contact pressure distribution for the indentation of the materials NBR, PU, PTFE+G, PTFE+kaolin+MoS_2 and TECAPEEK® for the normal loads of 9, 45, 90 and 135N. The **E**xperimental results are represented by **E** and those calculated by the **H**ertz **T**heory by **HT** followed by the respective applied load.

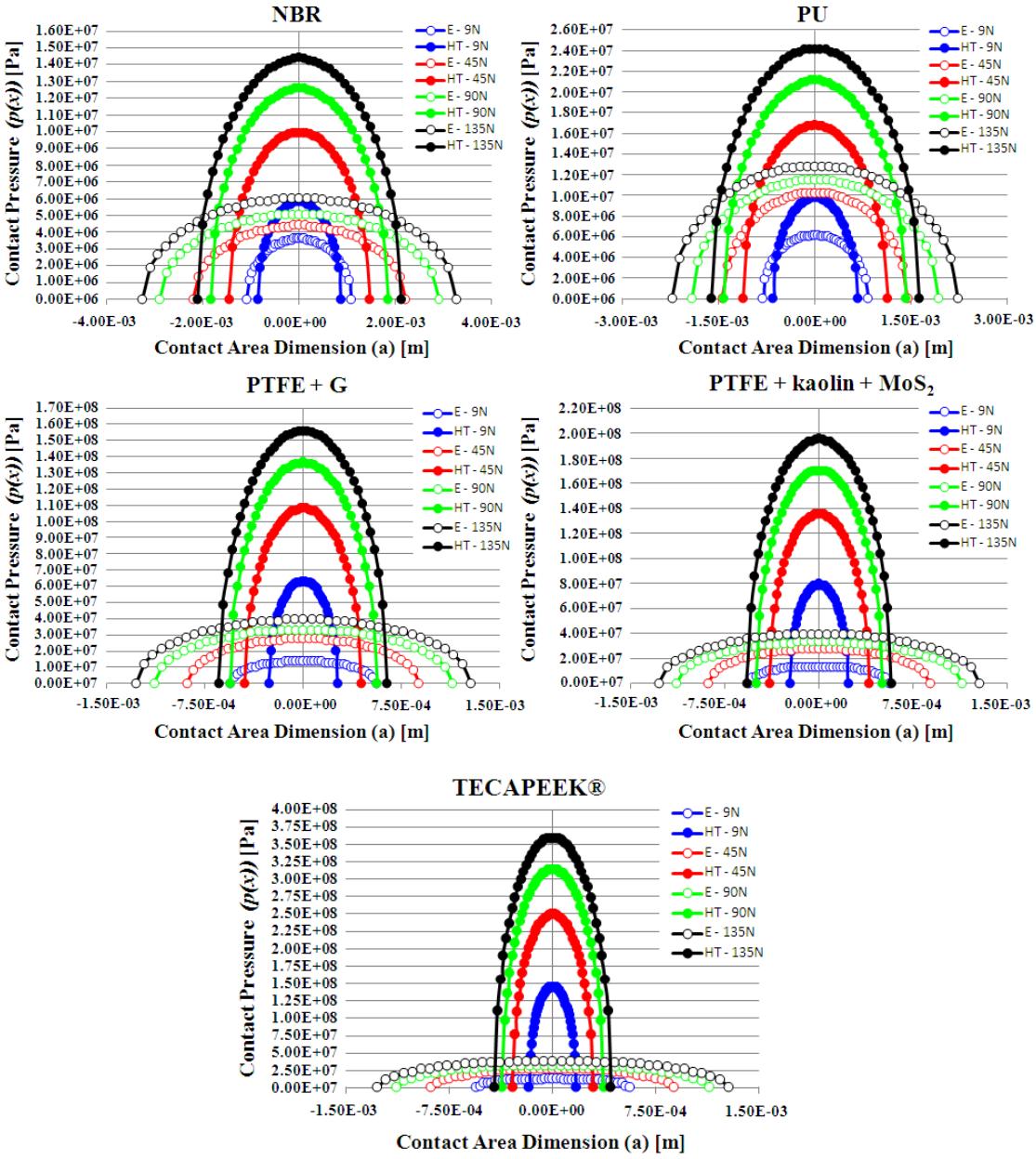

Figure 10. Theoretical (HT) and experimental (E) contact pressure distributions for the loads of 9N, 45N, 90N and 135N for NBR, PU, PTFE+G, PTFE+kaolin+MoS_2 and TECAPEEK®

Observing the graphs of the contact pressure distribution, it can be observed that the highest values of the contact pressure occurred for the polymeric composites, which present greater modulus of elasticity than the elastomers NBR and PU and, consequently, minor dimension of the contact diameter.

It can be also observed that the contact indentation diameter in the experimental results is well bigger than the theoretical results of Hertz that diminishes the contact pressure value. It suggests to be related with the fluency time and relaxation of the polymeric material, which internal structure begin to suffer a continuous deformation under the action of a constant normal load and, after an initial constant deformation, there is a tendency for the stress diminishes with the time. This is evidenced in the behavior of the variation of the contact pressure on these tested materials.

In the polymeric composites, the differences between the experimental and theoretical contact pressure distribution is well higher compared with the elastomers NBR and PU. TECAPEEK® presented the highest variation.

3.3. Shear Stress Distribution in the Hertz Contact Zone

Table 4 presents the results of maximum shear stress and its position with the depth (Hertz theory and experimental values) using the Equations **5b** and **6**. The results are distributed for the polymeric materials with the respective loads.

Table 4. Maximum Shear Stresses as a Normal Load function and its *locus* $\mathbf{z(\tau_{max})}$ with the depth for the materials **(a)** NBR, **(b)** PU, **(c)** PTFE+G, **(d)** PTFE+kaolin+MoS_2 and **(e)** TECAPEEK®

NBR			
Experiment		Hertz theory	
$\tau_{máx}$ [Pa]	$z(\tau_{máx})$ [m]	$\tau_{máx}$ [Pa]	$z(\tau_{máx})$ [m]
9N			
1.36E+06	*7.71E-04*	*2.19E+06*	*6.10E-04*
45N			
1.65E+06	*1.56E-03*	*3.74E+06*	*1.04E-03*
90N			
1.90E+06	*2.06E-03*	*4.71E+06*	*1.31E-03*
135N			
2.25E+06	*2.32E-03*	*5.39E+06*	*1.50E-03*

(a)

PU			
Experiment		Hertz theory	
$\tau_{máx}$ [Pa]	$z(\tau_{máx})$ [m]	$\tau_{máx}$ [Pa]	$z(\tau_{máx})$ [m]
9N			
1.64E+06	*5.43E-04*	*2.58E+06*	*4.33E-04*
45N			
2.70E+06	*9.46E-04*	*4.41E+06*	*7.40E-04*
90N			
3.03E+06	*1.26E-03*	*5.56E+06*	*9.33E-04*
135N			
3.39E+06	*1.46E-03*	*6.36E+06*	*1.07E-03*

(b)

PTFE+G			
Experiment		Hertz theory	
$\tau_{máx}$ [Pa]	$z(\tau_{máx})$ [m]	$\tau_{máx}$ [Pa]	$z(\tau_{máx})$ [m]
9N			
3.08E+06	*3.57E-04*	*1.42E+07*	*1.66E-04*
45N			
6.17E+06	*5.64E-04*	*2.43E+07*	*2.84E-04*
90N			
7.44E+06	*7.27E-04*	*3.06E+07*	*3.58E-04*
135N			
8.85E+06	*8.16E-04*	*3.51E+07*	*4.10E-04*

(c)

PTFE+ kaolin +MoS_2			
Experiment		Hertz theory	
$\tau_{máx}$ [Pa]	$z(\tau_{máx})$ [m]	$\tau_{máx}$ [Pa]	$z(\tau_{máx})$ [m]
9N			
2.52E+06	*3.50E-04*	*1.48E+07*	*1.45E-04*
45N			
5.32E+06	*5.40E-04*	*2.53E+07*	*2.47E-04*
90N			
6.84E+06	*6.73E-04*	*3.19E+07*	*3.12E-04*
135N			
8.12E+06	*7.57E-04*	*3.66E+07*	*3.57E-04*

(d)

TECAPEEK®			
Experiment		Hertz theory	
$\tau_{máx}$ [Pa]	$z(\tau_{máx})$ [m]	$\tau_{máx}$ [Pa]	$z(\tau_{máx})$ [m]
9N			
4.96E+06	*3.43E-04*	*4.38E+07*	*1.15E-04*
45N			
1.48E+07	*4.44E-04*	*7.48E+07*	*1.97E-04*
90N			
2.42E+07	*4.91E-04*	*9.43E+07*	*2.49E-04*
135N			
3.30E+07	*5.14E-04*	*1.08E+08*	*2.85E-04*

(e)

An appreciation about the values of the maximum shear stress and its respective *locus* $\mathbf{z(\tau_{max})}$ shown that it assumed an increasing distance of the contact interface when there was an increase of the load applied. The values of the shear stress *locus* are mainly dependants of the Poisson ratio $\boldsymbol{\nu}$ of the materials and the contact indentation diameter, **2a**.

With an increase of the material elasticity modulus (increase of the contact stiffness), it was verified a greater value of maximum shear stress and a higher proximity of the actuation *locus* of this stress telative to the contact interface. The shear stresses developed experimentally were smaller that the calculated from the Hertz theory and are observables mainly in the polymeric composites. The value of this stress and respective depth where it occurred, it were related with the contact indentation diameter, as higher this diameter smaller will be the value of operating shear stress and higher the *locus* where it occurs far from the contact interface. This can be sufficiently important in the study of material failures in a mechanical system that supports high static stresses.

Figure 11 shows the normalized shear stress distribution $(\tau/p_{máx})$ for the normalized depth (z/a) to the polymeric materials.

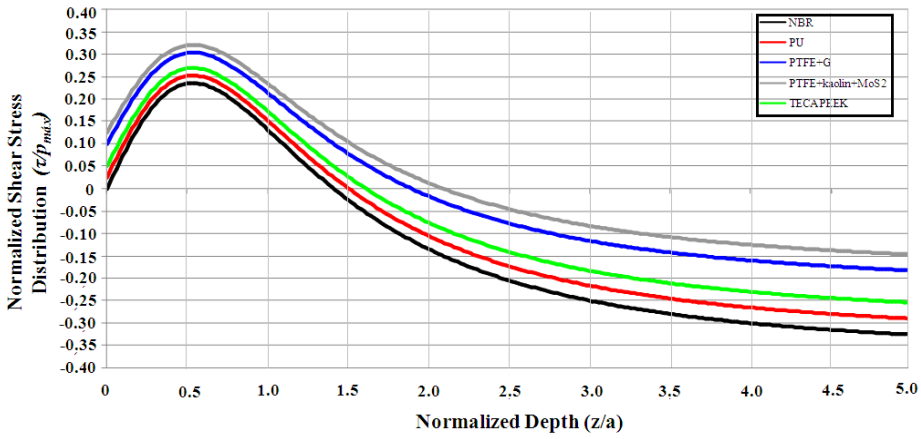

Figure 11. Normalized shear stress distribution versus the normalized depth to the tested polymeric materials.

For each material, the Hertz theory and experimental normalized shear stress distributions are identical, therefore the stress grow in the same ratios of the maximum pressure value that varies with the contact indentation diameter. The main responsible factor for the increase of the relation ($\tau/p_{máx}$) is the Poisson ratio ν of these materials – it is very important to perceive its relevance.

The maximum value of the relation $(\tau/p_{máx})$ was observed for the materials that presented a low Poisson ratio, ν. The measure that increased the Poisson ratio ν it diminished the maximum value of this relation next to the contact interface. The principal stresses produced by the action of the normal load induced to a shear stress that had its maximum value to a distance of the interface, for both the materials, of $z = 0{,}54\ a$, approximately.

Amongst the materials studied, the PTFE+kaolin+MoS_2, Poisson ratio ν = 0,25 presented the highest value of $(\tau/p_{máx})$ while the NBR, Poisson ratio ν = 0,5, presented the smaller value for this relation.

4. CONCLUSIONS

Comparing the results experimentally obtained and those calculated in accordance with the classic Hertz model of the Contact Mechanics, it has been demonstrated that this model necessity adjustments because it does not satisfy for the studied polymeric materials in contact with a steel spherical surface, mainly when the Hertz contact pressure assumes values of a magnitude of GigaPascal.

The influence of the behaviour viscoelastic of these polymers is evident in the results experimentally obtained in comparison with those correspondent theoretical values and mainly of the contact indentation diameters **2a**.

The composite polymeric matrices PTFE+G, PTFE+kaolin+MoS_2 and TECAPEEK® presented smaller differences between the experimental results and those calculated, what it could be observed through the contact indentation diameter results **2a** and respective curves of the contact pressure distribution.

5. ACKNOWLEDGES

The authors are thankful all that of some form had contributed since the beginning until the conclusion of this work with suggestions and critical that had enriched its content. In general, to all the integrant of the Group of Tribology Studies – GET-UFRN.

6. REFERENCES

HALE, Layton C. Appendix C: Contact Mechanics, in "Principles and techniques for designing precision machines." MIT ***PhD Thesis***, 1999. pp. 417-426.

HUTCHINGS, I.M. ***Tribology*** - Friction and Wear of Engineering Materials. Cambridge: British Library Cataloguing in Publication Data, 1992. 273p.

JOHNSON, K. L. ***Contact Mechanics***. Cambridge: Cambridge University Press, 1989. 452p.

MEDEIROS, J.T.N.; Fadiga de contato de discos metálicos não-conformes submetidos a ensaios a seco de rolamento cíclico. ***Tese de doutorado*** apresentada a Escola Politécnica em São Paulo, para obtenção do título de Doutor em Engenharia, 2002. 2 Vol.

NORTON, R.L. ***Machine Design*** . New Jersey: Prentice-Hall, 1996. 1048p.

PERSSON, B. N. J.; Contact Mechanics for Randomly Rough Surfaces, ***Surface Science Reports*** **61** (2006): 201-227.

STACHOWIAK, G.W.; BATCHELOR, A.W. ***Engineering Tribology***, 2005. 3rd ed. 832 p.

7. RESPONSIBILITY NOTICE

The authors are the only responsible for the printed material included in this paper.